Journal of Hydrology 620 (2023) 129294

Contents lists available at ScienceDirect

Journal of Hydrology

journal homepage: www.elsevier.com/locate/jhydrol

Research papers

Multicriteria land cover design via coupled hydrologic and multi-sector water management models

Tomasz Janus [a], James Tomlinson [a,b], Daniela Anghileri [c], Justin Sheffield [c], Stefan Kollet [d,e], Julien J. Harou [a,d,f,*]

[a] Department of Mechanical, Aerospace and Civil Engineering, The University of Manchester, Sackville Street, Manchester, M13 9PL, UK
[b] James Tomlinson Associates, Ltd, 81 Halmer Gate, Spalding, PE11 2EL, UK
[c] School of Geography and Environmental Science, University of Southampton, University Rd, Highfield, Southampton, SO17 1BJ, UK
[d] Institute of Bio- and Geosciences (IBG-3), Agrosphere, Forschungszentrum Jülich, Jülich, Germany
[e] Centre for High-Performance Scientific Computing in Terrestrial System, Geoverbund ABC/J, Jülich, Germany
[f] Department of Civil, Environmental & Geomatic Engineering, University College London, Gower Street, London, WC1E 6BT, UK

ARTICLE INFO

This manuscript was handled by S. Sally Elizabeth Thompson, Editor-in-Chief, with the assistance of Li He, Associate Editor.

Keywords:
Land cover design
Distributed hydrology
Multiobjective optimization
Multisector dynamics
Parallel computing

ABSTRACT

We investigate how hydrologic-land feedbacks and a hydrologic-water management linkage impact land cover arrangements optimized within a multiobjective land cover design framework. The framework integrates a spatially-distributed and physically-based hydrologic model, for simulating surface and subsurface flow and land processes, with a network-based multi-sector water resources management and allocation model. Both models used (Parflow, Pywr) are open-source. The framework is applied to a hillslope problem to identify land cover patterns that optimize trade-offs between water, food, energy and environment objectives. Results show trade-offs depend on land cover composition and the spatial arrangement of land covers within the catchment. Total runoff volume and peak flow of runoff was found to change 3 and 2-fold, respectively, between optimized solutions as land cover composition and spatial patterns were altered to satisfy different combinations of objectives. At the same time, up to a 15% reduction in the total runoff volume and an 8% reduction in the peak flow of runoff were observed within optimized land cover patterns having equal composition but different spatial arrangements. This emphasizes the impact on hydrologic behavior of the spatial location of land covers within a catchment. The emergence of patterns in land cover distribution for different trade-offs between objectives is driven by feedback mechanisms between subsurface hydrology and land processes, which are implicitly linked to the properties of each land cover and the interactions between neighboring land covers through lateral groundwater flow. The study demonstrates the added benefits of coupling distributed hydrologic models with water management simulation for multisector multicriteria land cover planning.

1. Introduction

Vegetation influences the energy and moisture fluxes between land, atmosphere and subsurface via (1) net radiation, (2) evaporation and transpiration, (3) interception of rainfall and (4) redistribution of moisture via root water uptake (Maxwell and Miller, 2005; Kuffour et al., 2020). As a result, catchments with the same geomorphology but with varying land cover are likely to exhibit different local climatic properties, such as diurnal temperature ranges, as well hydrologic conditions on top of and below the surface (Siriwardena et al., 2006; Mao and Cherkauer, 2009). Ultimately, land cover and its spatial arrangement affects water resource availability in river basins thus impacting different sectors such as food and energy production as well as other environmental services (D'Odorico et al., 2018). Informing land cover decisions is therefore a multiobjective problem because different sectors use the same resources and thus, may be in conflict. The task is additionally complicated by the complex nature of the interactions between land, atmosphere and the subsurface (Dai et al., 2003). Assisting land cover decision-making with computational models may therefore provide unreliable guidance if these models are unable to describe those interactions with sufficient level of fidelity. On the other hand, detailed and thus computationally expensive mechanistic models are likely to generate high computational overheads which might render them inapplicable in decision making frameworks. However, recent advancements in the accessibility and the affordability

* Corresponding author at: Department of Mechanical, Aerospace and Civil Engineering, The University of Manchester, Sackville Street, Manchester, M13 9PL, UK.
E-mail address: julien.harou@manchester.ac.uk (J.J. Harou).

https://doi.org/10.1016/j.jhydrol.2023.129294
Received 22 August 2022; Received in revised form 23 December 2022; Accepted 15 February 2023
Available online 8 March 2023

of high performance computing (HPC) combined with parallelization of numerical solvers, e.g. Richards et al. (2005), Kollet and Maxwell (2006), Shen and Phanikumar (2010) enable gradual introduction of rigorous physically-based simulation models into quantitative decision making frameworks. Another barrier to overcome, when it comes to mechanistic hydrologic models, is the increased number of parameters and measurements required for their identification in comparison to simpler e.g. behavioural models. Under a shortage of a sufficient amount and quality of calibration data, we may end up with models with potentially large prediction uncertainty even though they are more physically sound. This topic, although not the subject of this discourse, has been addressed in great detail in Beven (2007, 2019).

Hydrologic models range from lumped (Siriwardena et al., 2006; Delgado et al., 2010; Tong et al., 2012), to semi-distributed (McColl and Aggett, 2007; Hundecha and Bárdossy, 2004; Choi and Deal, 2008; He and Hogue, 2012) and distributed (Kollet and Maxwell, 2008; Mao and Cherkauer, 2009; Wijesekara et al., 2012; Condon and Maxwell, 2013; Mikkelson et al., 2013; Penn et al., 2016; Bearup et al., 2016; Markovich et al., 2016) and can be implemented within domains of different sizes from hill-slopes (Mikkelson et al., 2013; Penn et al., 2016; Bearup et al., 2016; Markovich et al., 2016) to whole catchments (Hundecha and Bárdossy, 2004; Siriwardena et al., 2006; McColl and Aggett, 2007; Choi and Deal, 2008; Kollet and Maxwell, 2008; Mao and Cherkauer, 2009; Delgado et al., 2010; He and Hogue, 2012; Tong et al., 2012; Wijesekara et al., 2012). The cited studies report strong links between land cover and hydrologic characteristics of a watershed and water budgets, e.g., total overland flow and evapotranspiration (ET), as well as its dynamic response, e.g., short- and long-term storage and memory. Hundecha and Bárdossy (2004) observed a reduction in peak runoff and total runoff volume resulting from afforestation. Tong et al. (2012) concluded that the already prominent impacts of land cover change on the quantity and quality of water resources are further amplified under climate change. Choi and Deal (2008), He and Hogue (2012) investigated the impacts of urbanization on water resources using a semi-distributed hydrologic model with land cover types having aggregated vegetation and soil permeability characteristics and concluded that urbanization caused decreased base flow and groundwater recharge in the watershed. Wijesekara et al. (2012) demonstrated long-term impacts of land cover changes on hydrologic processes in a watershed in Canada. Öztürk et al. (2013) used the model developed by Wijesekara et al. (2012) to conclude that the water budget was most sensitive to variations in precipitation and conversion between forest and agricultural lands. Julian and Gardner (2014) reported that the characteristics of runoff patterns also depend on the watershed scale with small watersheds being driven by precipitation whilst bigger watersheds being more dependent on watershed processes such as short and long term storage and memory. However, these studies did not report on (a) how watershed hydrology is also dependent on spatial configurations of land cover within the catchments nor (b) on which processes drive the spatially distributed interactions between land cover and hydrology.

The latter of the two above research questions has been explored in several other studies performed with detailed mechanistic models providing physical description of surface and subsurface hydrology and vegetation-dependent energy fluxes on the land surface using 2D hillslope models. These studies demonstrated the complexity of how vegetation interacts with soil and atmosphere. Consequently, a compelling case was made for advancing integrated land cover-hydrologic modelling frameworks via replacement of conceptual models with mechanistic models that can describe the intricate processes governing the interactions between the surface and the subsurface. Some of the notable findings of those studies are described below. Kollet and Maxwell (2008) applied a 3D variably saturated groundwater flow model ParFlow (Ashby and Falgout, 1996; Jones and Woodward, 2001) coupled with the Common Land Model (CLM) (Dai et al., 2003) to study connections between groundwater dynamics and land surface energy balance components and demonstrated a strong coupling between a number of energy variables and the time-varying water table depth (WTD). The authors found a critical WTD range, related to vegetation root depth, where a strong coupling exists between groundwater and land-surface processes. Kollet and Maxwell (2008) reported that, additionally, soil heterogeneity had a strong influence on ET during dry periods in which ET became limited by moisture in the shallow subsurface. Markovich et al. (2016) applied the same model to alpine hillslopes and found that the responses were sensitive to the unsaturated zone retention parameters, which in the case of alpine systems could indicate a mix of matrix or fracture flow. The inter-connectivity between groundwater and land processes was further explored in the context of water management by Condon and Maxwell (2013) who connected an optimization-driven water allocation model to ParFlow. The study demonstrated the added benefits of fully integrated water management tools on a case study where spatial and temporal variability in soil moisture predicted in the hydrologic model drove water allocations for irrigation.

Hydrologic and land use models were also embedded within multi-objective optimization frameworks. The results showed trade-offs between different bundles of land use decisions and water-related objectives. However, the number of such studies to date have been limited and focused on agricultural applications. One of the notable studies was done by Lautenbach et al. (2013) who investigated optimal trade-offs between biodiesel production, food crops production and water quality and quantity on a catchment level using the integrated river basin model SWAT (Arnold and Fohrer, 2005) connected to NSGA-II (Deb et al., 2002) multiobjective evolutionary algorithm. Fowler et al. (2015) created a multiobjective optimal decision making framework for selecting crop types in a watershed using the MODFLOW groundwater flow model integrated with supply-and-demand components of irrigated agriculture in order to maximize revenue, minimize water use and maximize demand satisfaction. The authors found optimal trade-offs between the objectives and calculated the respective areas of each of the three crop types for each trade-off. The above two studies demonstrated the benefits of multi-objective optimization with coupled hydrologic-land models. These studies described land use allocation with macroscopic quantities such as fractions of area per individual land use type or type of land use per cell. What the studies were not able to demonstrate is how these different land uses should be spatially arranged within catchments, due to the limitations imposed by the hydrologic-landuse models being used. The need for sophisticated hydrologic models in land use optimization was suggested by He and Hogue (2012) who stated that land use decision making requires hydrologic models that consider spatio-temporal watershed characteristics due to their capacity of enabling more accurate prediction of dynamic water balances in a watershed.

Among the most recent developments, Sheikh et al. (2021) attempted a multiobjective land use optimization with a distributed hydrologic model on a catchment scale and reported impact of land use patterns on surface runoff and sediment load. Several recent papers approached water energy food (WEF) nexus studies with multiobjective optimization methods complemented with different methodological improvements. For example, Guo et al. (2022) used a distributed multi-objective uncertain optimization model to develop comprehensive strategies for agricultural sustainability whilst handling stochastic and fuzzy uncertainties. Yue et al. (2021), Li et al. (2022), Ren et al. (2022) performed WEF nexus studies using multiobjective optimization. The first two addressed uncertainty through adoption of LR-type fuzzy numbers, and Me-measure fuzzy chance-constrained programming, respectively, whilst (Ren et al., 2022) introduced objectives quantifying long-term life cycle. A notable paper was recently published by Yang et al. (2023) who used surrogate neural network models to leverage computational burden of storm water management models in multiobjective optimization applications. It is likely that in the

near future, more researchers will adopt such approaches, especially in combination with explainable deep learning techniques (Ras et al., 2020) in order to keep computation within feasible time bounds whilst, at the same time, addressing problem of greater scale.

To our knowledge no study has assessed the impact of feedbacks between land and the subsurface on the spatial land cover patterns recommended by multi-objective landcover optimization. We used a land cover design framework that links a distributed mechanistic hydrologic and land surface model with a multi-sector water management model and connects the two to a multiobjective evolutionary algorithm (MOEA). For a description of MOEA and multiobjective design, we refer the reader to Deb (2001), Reed et al. (2013). The framework allows finding spatial land cover designs that lead to optimal trade-offs between multiple competing objectives. We show how the spatial optimized land cover selections change as preferences between performance measures are shifted. Our aims are (a) to demonstrate how spatial land cover allocation decisions under competing objectives are influenced by bi-directional interactions between land surface processes and groundwater dynamics, and (b) to assess which of these processes have the largest influence on land management decisions. We show that water table depths affect evapotranspiration differently depending on the vegetation type which has different root depths, leading to distinct trade-offs between land cover patterns for different objectives related to water, energy, food and environment.

2. Methods

The flowchart visualizing how the distributed hydrologic model, the water resources model and the multiobjective optimization algorithm are connected, is shown in Fig. 1. The hydrologic model produces runoff as a response to atmospheric forcing and as a function of hydrologic parameters and land cover allocation. The runoff becomes an input to the water resources model creating a one-way interaction between both model components. It is also possible to create a two-way closed-loop interaction by making decisions in the water resources model such as water abstractions that become sink terms in the hydrologic model (dashed arrow in Fig. 1). The selected outputs and state variables from both models are used to formulate design criteria which become objective functions for the multi-objective optimization algorithm. Because objectives are conflicting, improvement of one objective causes deterioration of at least one other objective. Therefore, the optimizer searches not for a single optimal land cover allocation (solution) but for the set of Pareto optimal solutions. A solution is said to be Pareto optimal or nondominated, if none of the objectives can be improved without degrading some of the other objectives. To ensure that the results are close to the true Pareto surface, i.e. a global set of optimal solutions is found, the optimization procedure is initialized from multiple starting points (seeds). Those individual sets of nondominated solutions are filtered to produce a portfolio of optimal land cover configurations, which can be further explored in different contexts related to the different objectives.

2.1. Theoretical background

On the land surface, mass and heat exchange processes driving the watershed hydrology are dependent on land cover and on groundwater levels, as conceptually described in Fig. 2. The schematic is borrowed from Kollet and Maxwell (2008) who divided the hillslope into three zones characterized by the availability of water for evapotranspiration at the land surface. The schematic illustrates, from a conceptual point of view, why watershed hydrology is dependent on spatial configurations of land covers and consequently, why distributed hydrologic and land models may be required in multi-criteria land cover and land use design. The rates of evapotranspiration (ET) change with groundwater levels differently for different types of vegetation as a result of an interplay between water availability and rooting depth. In Zone 1, the water table is shallow and ET is never water-limited. In Zone 2, access to groundwater by some of the vegetation types such as crops or grass having shorter root depths become water limited whilst biological activity of other vegetation types such as trees remains not water-limited. In Zone 3, groundwater is deep and thus disconnected from the land surface, resulting in land processes being less dependent on subsurface hydrology. A more thorough explanation of the influence of groundwater dynamics on land surface processes in a distributed coupled hydrologic-land model can be found in Kollet and Maxwell (2008).

2.2. Computational implementation

The multiobjective optimization framework proposed in this paper was implemented by connecting two standalone models into an integrated simulator: (a) a distributed variably saturated groundwater flow simulator ParFlow (Ashby and Falgout, 1996; Jones and Woodward, 2001) coupled with a land surface model CLM (Dai et al., 2003; Oleson et al., 2010) (b) a free open-source Python-based water resources modelling library Pywr (Tomlinson et al., 2020). The code for connecting Pywr with ParFlow is written in Python. In each simulation run, ParFlow is called as an external process from within Python using `subprocess.run`. After successful execution of the ParFlow model, runoff time-series are extracted from ParFlow's output files. Pywr, which is written in Python, is then executed using the extracted runoff data as input. The simulation environment for sequential execution of ParFlow and Pywr is wrapped by the wrapper class that facilitates exchange of data between both models and the MOEA algorithm. In each model evaluation, MOEA receives objective function values from both models and sets the configuration of land covers which are then written into Parflow's land cover input file using Jinja templating engine (Jinja Templating Engine, 0000).

2.2.1. ParFlow/CLM

ParFlow/CLM models variably saturated subsurface flow with overland flow (Kollet and Maxwell, 2006) in a fully coupled manner and captures the functional relationships between groundwater dynamics and water and energy fluxes on land surface (Maxwell and Miller, 2005; Kollet and Maxwell, 2008) by replacing the soil column/root-zone soil moisture formulation in CLM with the ParFlow formulation leading to more realistic behaviour that more closely matches observations (Maxwell and Miller, 2005). ParFlow implements Richards' equation for variably saturated 3D subsurface flow and shallow water equations for surface flow. The capabilities of ParFlow to simulate coupled surface–subsurface flow are described in detail in Kuffour et al. (2020). CLM models vegetation processes describing energy and water exchange between surface and atmosphere as plant function types specified by optical, morphological and physiological properties. CLM accounts for the thermodynamic equilibrium of the soil air at the interface with the matrix potential and turbulent transport based on the Monin–Obukhov similarity theory (Monin and Obukhov, 1954). The phenological states of vegetation types e,g, the growth phase and the ripening phase of crops, are simulated via the leaf area index (LAI) and steam area index (SAI) based on their maximum and minimum values and an empirical parameterization resulting in time varying evapotranspiration over the growing season. The root density distribution in the subsurface is modelled with a sum of exponential functions and is uniquely parameterized for different land cover types. A detailed description of the land processes included in the ParFlow's CLM implementation can be found in Maxwell and Miller (2005).

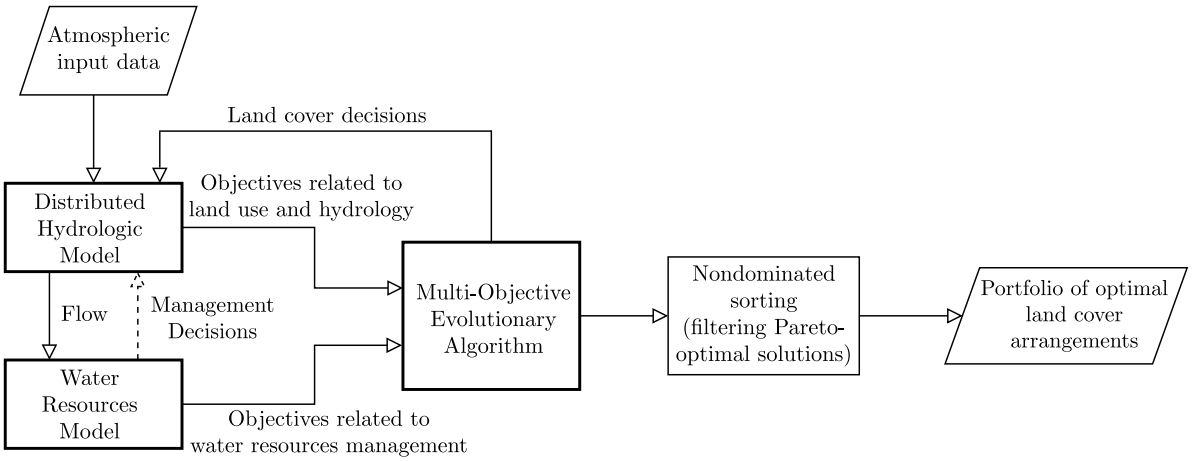

Fig. 1. Flowchart of the proposed approach for multi-criteria optimized land cover design using a distributed hydrologic-land model and a distributed water resources model. Parallelograms indicate inputs and outputs. Dashed arrow indicates feedback connection from the water resources model to the hydrologic model which the framework enables but which has not been explored in the case study.

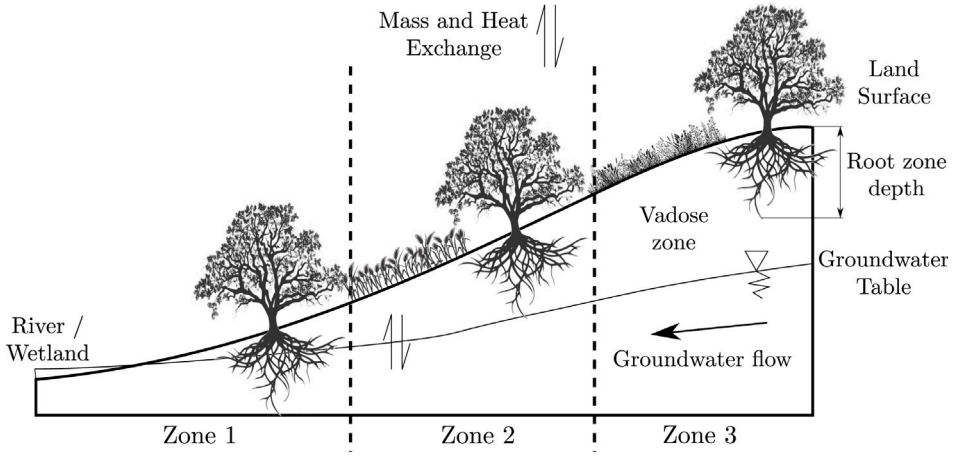

Fig. 2. Schematic of a hillslope borrowed from Kollet and Maxwell (2008) showing a typical groundwater table depth profile in relation to surface elevation indicating three distinct zones with shallow (Zone 1), intermediate (Zone 2) and deep (Zone 3) groundwater levels with regards to root zone depth. The root zone depth is not drawn to scale and the groundwater table profile is drawn arbitrarily.

2.2.2. Pywr

Pywr (Tomlinson et al., 2020) is a model library for the simulation of managed water resource systems. It uses a linear-programming formulation to simulate least cost water allocations at each simulation time-step as a function of allocation penalties, rules and constraints. In this case study, Pywr is used for calculating water mass balances in a hydroelectric reservoir, the extent of flooding in a stretch of the river connecting runoff from the hillslope to the hydroelectric reservoir, and the amount of HP generated in the hydroelectric reservoir.

2.3. Case study

The conceptual multi-sector human-natural system design problem described in this paper is applied to a simple synthetic system. Five conflicting socioeconomic dimensions are implemented in the multi-objective optimization. The water resources dimension is represented with two objectives: (1) related to the propensity of the system to flood, and (2) related to total annual runoff volume. The latter quantity correlates with hydropower production in the hydroelectric reservoir. (3) The second energy dimension is solar power potential which is set to be proportional to the area of bare soil in the catchment. It is assumed that land surface underneath solar panels in our hypothetical semi-arid area (see Section 2.3.3) will eventually become barren due to lesser availability of sunlight and elevated levels of heat. (4) The food production dimension is approximated by the area of the catchment covered with rain-fed agriculture. (5) A proxy for ecosystem health quantifies the number of distinct land cover types within the catchment excluding bare soil.

2.3.1. Case study model structure

The structure of ParFlow/CLM and Pywr models implemented in the case study and the connections between the models and the multiobjective evolutionary algorithm (MOEA) are visualized in a block diagram in Fig. 3.

The computational domain of ParFlow/CLM is a 2D hillslope, which simplifies the analysis and interpretation of results compared to a 3D catchment, especially with regards to the relationships between lateral subsurface flow, WTD and ET, by removing one spatial dimension, whilst still retaining the required subsurface flow complexity. The hillslope is divided into ten cells indexed from 0 to 9. The model interacts with the atmosphere via bi-directional exchange of the energy and water mass fluxes at the land surface and is linked with the upstream parts of the catchment via base flow q_b. The terrain has a slope that is sufficiently large to induce groundwater limited conditions in the upstream sections of the hillslope.

The Pywr water allocation model is represented by a graph of connected nodes with directed edges representing transfers of water between the nodes following set rules and priorities. The city node

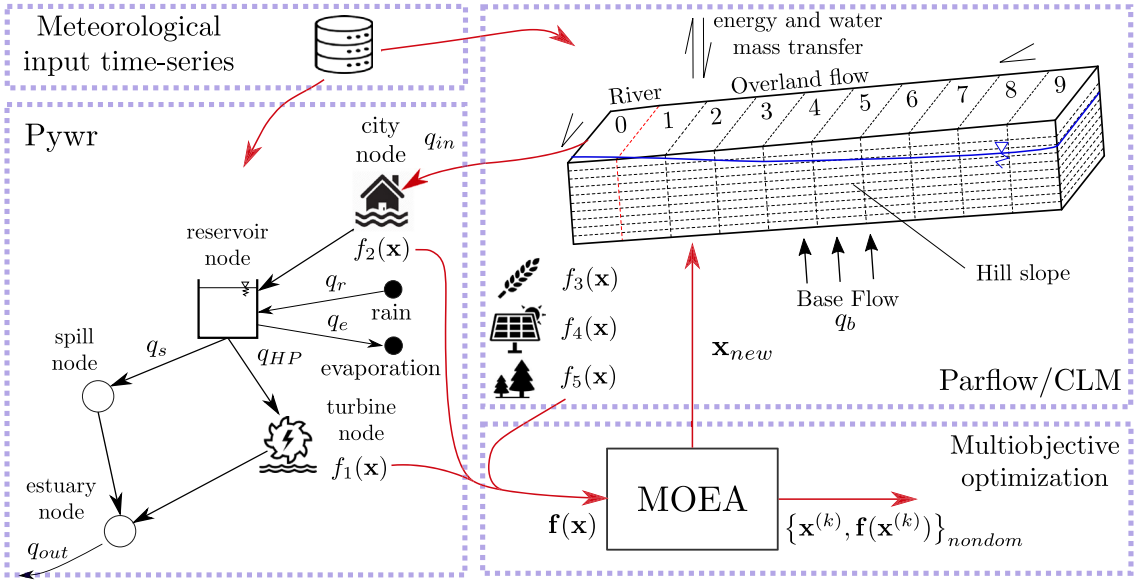

Fig. 3. Block diagram describing the structure and the flow of information between all components of the multi-criteria land cover design model implemented in the case study.

representing a river section with a weir is modelled as a long shallow trapezoidal reservoir with an overflow. The amount of overflow is proportional to $h^{0.5}$ where h is the height of water above the weir. The inclined sides of the reservoir represent the river banks. The reservoir node models a hydroelectric reservoir which stores and directs the water to a hydropower turbine node. The turbine node calculates the generated hydroelectric energy as a function of water volume and the difference between turbine elevation and water level in the reservoir node. The flow of water q_{HP} is allocated to the turbine node in every time step following a release control curve that defines the relationship between q_{HP} and the volume of water in the reservoir V. In case the volume of water exceeds the reservoir's capacity and the calculated release exceeds the maximum allowed throughput of the turbine, the excess water q_s is directed to the estuary via the spill node. The rain and the evaporation nodes model the additional sources and sinks of water due to precipitation q_r and evaporation q_e from the water surface, respectively. Rain and evaporation nodes do not feature in the city node due to its small surface area and thus, negligible effects of surface-dependent rain and evaporation processes on the overall water mass balance. The rain source q_r and evaporation sink q_e are derived from the meteorological input time-series that drive the hydrologic response of ParFlow/CLM. q_r is calculated directly from rainfall whilst q_e is computed using the Penman–Monteith equation (Penman and Keen, 1948; Allen, 2005). The input q_{in} to Pywr is equal to the daily average of the hourly runoff time-series output from ParFlow/CLM. After every simulation (model evaluation) of the coupled ParFlow/CLM-Pywr model values of all five objective functions $f_i(\mathbf{x})$ (see next section) are calculated and passed to the MOEA as a vector $\mathbf{f}(\mathbf{x})$. In each iteration, MOEA adjusts the 10×1 input vector $\mathbf{x}$ of land cover types and passes the updated sequence $\mathbf{x}_{new}$ to Parflow/CLM.

2.3.2. Optimization implementation

Out of five objectives three are calculated in ParFlow/CLM: number of cells with crops f_3, number of cells with bare soil f_4, and land cover diversity f_5. The remaining two objectives, i.e. annual hydropower production f_1, and flood extent f_2, are calculated in Pywr in the turbine and in the city node, respectively. The multiobjective optimization problem (MOP) is formulated as follows:

$$\max_{\mathbf{x}} \ \mathbf{f}(\mathbf{x}) = \left\{ f_1(\mathbf{x}), f_2(\mathbf{x}), f_3(\mathbf{x}), f_4(\mathbf{x}), f_5(\mathbf{x}) \right\} \ \ \mathbf{x} \in \Omega \tag{1}$$

where Ω denotes the solution space, i.e. all possible land cover configurations in the hillslope, $f_i(\mathbf{x})$ denotes the ith objective function and $\mathbf{f}(\mathbf{x})$ denotes the set of all objective functions for solution $\mathbf{x}$. $\mathbf{x}$ is represented as a 10×1 vector in which each element x_j, for $j = 0, \ldots, 9$, defines the type of land cover allocated to the jth cell. The land cover type is encoded as an integer value, i.e. $x = 0$ for mixed forests, $x = 1$ for grasslands, $x = 2$ for croplands and $x = 3$ for bare soil. The mixed forest type in CLM is parameterized to represent a mixture of coniferous, deciduous and evergreen broad-leaved species. Grasslands and croplands represent vegetation types with short root depths (RDs). The five objective functions are defined as follows:

$$f_1(\mathbf{x}) = 2.4 \times 10^{-7} \sum_{k=1}^{365} \eta_t \, \rho \, g \, q_{HP}^k(\mathbf{x}) \left(H^k - z_T \right) \tag{2}$$

where q_{HP}^k and H^k are, respectively, flow rate through hydropower turbine and water level in the hydroelectric reservoir in kth daily timestep, z_T is the turbine elevation, η_t is the turbine's total efficiency, ρ is the water's density and g is the gravitational constant. 2.4×10^{-7} is the conversion coefficient required to obtain hydropower production in MWh assuming that all variables in the hydropower equation on the right side of the summation symbol are given in SI units. The flow released from the reservoir to the turbine $q_{HP}^k = f_{HP}\left(V_{HP}^k\right)$ is calculated for each timestep in Pywr using a piecewise linear release curve f_{HP} relating the released flow to the volume of water in the reservoir.

$$f_2(\mathbf{x}) = \max_k \left(-1 \times A_{flood}^k(\mathbf{x}) \right) \quad \forall k \in \{1, \ldots, 365\} \tag{3}$$

The flooded area in kth timestep A_{flood}^k is multiplied by -1 to minimize the extent of flooding since the problem is posed as a maximization problem. A_{flood} is calculated in the city node using a bathymetric curve $A_{flood}^k = f_{flood}\left(V_{city}^k\right)$ where $f_{flood}(\cdot)$ is a function derived from geometric dimensions of the reservoir and V_{city}^k denotes the volume of water stored in the city node in kth timestep.

Using Iverson bracket notation

$$f_3(\mathbf{x}) = \sum_{x \in \mathbf{x}} [x = 2] \tag{4}$$

calculates the number of cells in solution $\mathbf{x}$ allocated to rain-fed croplands, which are coded in the algorithm with integer number 2. Similarly,

$$f_4(\mathbf{x}) = \sum_{x \in \mathbf{x}} [x = 3] \tag{5}$$

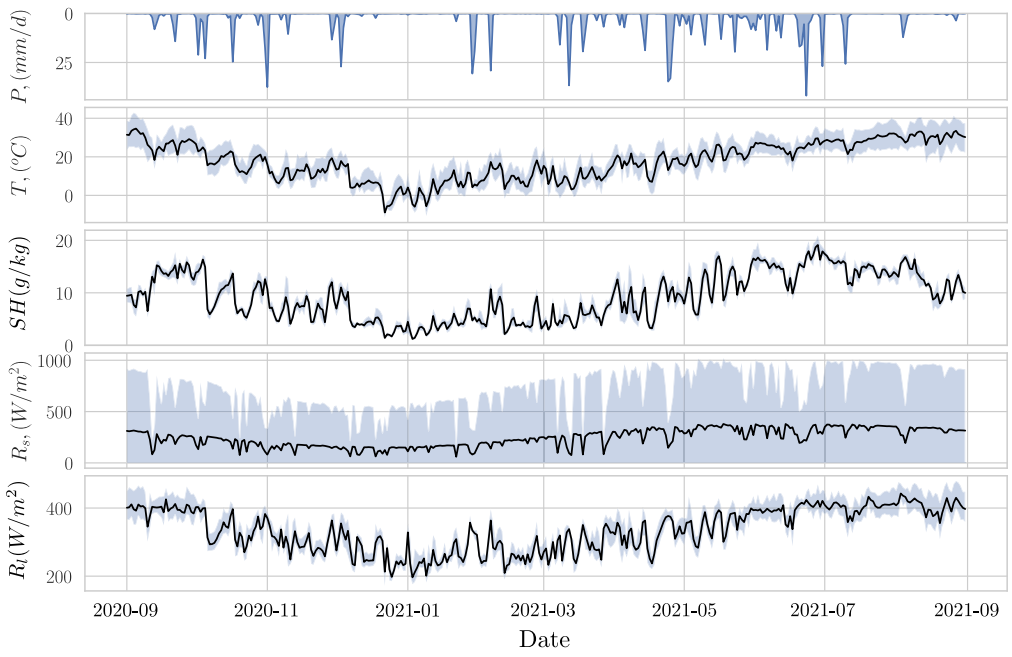

Fig. 4. Time-series of daily-average values (black solid line) and hourly variations (blue shaded area) of the selected meteorological variables. From top to bottom: precipitation P, temperature T, specific humidity SH, short-wave radiation R_s and long-wave radiation R_l.

describes the number of cells in solution **x** allocated to bare soil.

$$f_5(\mathbf{x}) = \text{card}\left(\{x \in \mathbf{x} \mid x \neq 3\}\right) \tag{6}$$

where $\text{card}(\{\cdot\})$ denotes cardinality of a set, models land cover diversity as a number of unique land cover types in the solution **x** excluding bare soil.

For this search-based design application, we used a dominance based many objective evolutionary optimization algorithm called NSGA-III (Deb and Jain, 2014; Jain and Deb, 2014).

2.3.3. Model inputs and parameters

Five important meteorological variables out of 8 variables in total that form the input to ParFlow/CLM-Pywr are plotted in Fig. 4. Due to high computational complexity of our study imposed by ParFlow/CLM and MOEA, the input timeseries were limited to a single year at an hourly time-step. The meteorological inputs are representative of a subtropical semi-arid zone. This setting is chosen to allow testing the sensitivity of land and subsurface interactions in an environment exhibiting high variability in atmospheric conditions such as inter- and intra-day temperatures and solar irradiation as well as sporadic precipitation patterns with periods of droughts. Catchments in semi-arid zones are characterized by high temporal variability of various hydrologic variables that drive the processes on the land surface, such as soil moisture content and water table depth (WTD). Consequently, the vegetation-driven energy fluxes at the surface may vary significantly in response to changes in evapotranspiration, throughfall and infiltration, thus having an impact on subsurface hydrology. Based on this setting, we are able to test the model's behaviour under a range of conditions with ET intermittently limited by shallow soil moisture deficits and with seasonal water shortages affecting water table levels. We shall see that as table level depths affect ET differently depending on the vegetation type, as illustrated conceptually in Fig. 2, interesting tradeoffs emerge between land cover patterns for different objectives.

The plotted variables, from top to bottom are: precipitation P, temperature T, specific humidity SH, short-wave radiation R_s and long-wave radiation R_l. The catchment is characterized with high shortwave radiation with an average annual value of approximately 300 W/m^2 and slight and moderate rainfall throughout the year with longer dry periods in the winter months. The temperature in degrees Celsius ranges from high and mid 30s in summer months to small negative values in winter months, with an annual average of approximately 18°C. Humidity, when converted from specific to relative, ranges between 30% and 85% depending on the period of the year. The hillslope also receives base flow $q_b = 120$ m^3/d equivalent to flux $v_b = 0.0288$ m/h uniformly distributed along the bottom boundary of the hillslope. Base flow represents groundwater contribution from hypothetical upstream sections of a larger catchment within which our study is situated.

The parameters of ParFlow, CLM and Pywr models are listed in Table 1. The hydraulic conductivity is representative of typical medium to coarse sands whose hydraulic coefficients range between 3×10^{-4} m/h and 1.8 m/h for medium sands, and 22 m/h for coarse sands. The porosity is in the upper end of values for sandy soil types whose porosities typically lie between 0.25 and 0.50. Soil heterogeneity was not modelled in order to allow easier interpretation of final results. The Manning's coefficient $n_h = 0.20$ s/m$^{1/3}$ set for the hillslope is representative of forests and shrublands whilst $n_r = 0.03$ s/m$^{1/3}$ set for the river section is characteristic of coarse-sand river bed (Arcement and Schneider, 1989). The parameters of the CLM model listed in Table 1 were assigned default values set in ParFlow/CLM (Maxwell and Miller, 2005). Vegetation classes implemented in ParFlow/CLM follow IGBP land cover type classification (IGBP, 0000) and additionally include an additional land cover type representing bare soil. The parameters of all vegetation classes are provided as supporting data in file `drv_vegp.dat`. The relationship between the volume and the water level, as well as the water surface area for the hydroelectric reservoir are provided in two bathymetric curves $h = h(V)$ and $A = A(V)$. For a vector of volumes $V = (0, 14650, 29301, 43951, 58602, 73252, 87903, 102553)$ m^3, $h(V) = (0, 5, 10, 15, 20, 25, 30, 35)$ m and $A(V) = (1875, 2150, 2440, 2743, 3062, 3394, 3741, 4102)$ m^2.

2.3.4. Computation

The optimization algorithm NSGA-III (Deb and Jain, 2014; Jain and Deb, 2014) was implemented in a framework for evolutionary computing in Python, called Platypus (Hadka, 2015). Parallelization support in Platypus allowed us to perform the study on multiple computer nodes using message parsing interface (MPI) with Python's native `mpi4py` (MPI4PY, 0000). All simulation and optimization runs were

Table 1
Parameters of the integrated ParFlow/CLM and Pywr model.

Parameter		Value	Unit
	ParFlow		
Domain geometry (l_x, l_y, l_z)		1000, 100, 10	m
Number of cells (n_x, n_y, n_z)		10, 1, 10	–
Slope of the hillslope section (S_h)		0.03	–
Slope of the river section (S_r)		0.001	–
Saturated hydraulic conductivity (K_s)		1	m/h
Porosity (ϕ)		0.415	–
Van Genuchten parameters (α, n)		1, 2	1/m, –
Residual saturation (S_r)		0.2	–
Specific storage (S_s)		1.0×10^{-4}	1/m
Manning's coefficient on the hillslope (n_h)		5.52×10^{-5}	h/(m$^{1/3}$)
Manning's coefficient on the river bed (n_r)		8.333×10^{-6}	h/(m$^{1/3}$)
	CLM		
Maximum allowed dew (dewmx)		0.1	mm
Soil layer thickness discretization (scalez)		0.025	m
Length scale for K_s decrease (hkdepth)		0.5	m
Fraction of model area with high water table (wtfact)		0.3	–
Max transpiration for moist soil (trsmx0)		10.0	mm/s
Wilting point potential (smpmax)		-1.5×10^5	mm
Roughness length for soil (zlnd)		0.01	m
Roughness length for snow (zsno)		0.0024	m
Drag coefficient for soil under canopy (csoilc)		0.004	–
	Pywr		
Maximum reservoir volume (V_{max})		102553	m^3
Water level at maximum fill (H_{max})		35	m
Turbine elevation (z_t)		1	m
Turbine efficiency (η_t)		0.85	–
Reservoir control rule:	flows ($\mathbf{q}_{HP}$)	0,150,400,1000,2000,3500	m^3/d
	volume fractions:	0.0,0.2,0.4,0.6,0.8,1.0	–

conducted on a high performance computing (HPC) cluster hosted at the University of Manchester. The study was run on 144 cores using high performance nodes of 2 × 12-core Intel Xeon E5-2690 v3 @ 2.60 GHz + 128 GB RAM. Parallelization was implemented by dividing the population of candidate solutions inside the genetic algorithm (GA) into isolated islands of sub-populations. Evaluation of each population member required a simulation of one instance of the integrated ParFlow/CLM-Pywr model. Each simulation was run for the duration of 3 physical years repeating the one-year-long meteorological input. First two years of the simulation were used to attain an approximation of a dynamic equilibrium. The results obtained in the third year of the simulation were used to calculate the objectives. Each simulation run was started with the same set of initial conditions. Optimization was started from 5 randomly generated initial populations (seeds) of size 132 with 140,000 function evaluations per seed. The running time of each optimization per seed was approx. 7 days. At the end of all five optimization runs, non-dominated sorting was performed on the nondominated solutions collected from all five seeds. The final result is a Pareto-optimal surface composed of 145 nondominated solutions.

A 2-year spinup was sufficient to attain 1% convergence in land surface variables, i.e. latent, sensible and ground heat fluxes, upward long-wave radiation, ground surface temperature and bottom layer temperature. Convergence criterion is set as annual relative difference between output variables/states in consecutive years. These results are in agreement with the studies of Ajami et al. (2014), Seck et al. (2015) which were based on ParFlow/CLM and reported that 2, 9, 6 and 5 years of spin-up were sufficient to achieve 1% convergence between start and end day of a year-long simulation in groundwater (GW) storage, unsaturated storage, and water storage within CLM model and root zone, respectively. Restricting the simulation to 1 physical year following a 2-year spinup, was required due to (a) significant execution times of ParFlow/CLM and (b) $\mathcal{NP}$-hard complexity of the combinatorial optimization problem at hand Serafini (1987).

3. Results and discussion

The results are presented and discussed in three subsections. (1) We provide plots illustrating tradeoffs between the multiple objectives of our hypothetical land cover design problem. These plots convey information about the impact of land cover selection on different multi-sector services. (2) We illustrate the spatial land cover patterns generated by the optimization results which show how catchments with the same aggregate land cover composition but with different spatial distributions exhibit different hydrologic behaviour. (3) We discuss which hydrologic and land processes have the largest impact on land cover selection and present the argument for wider application of distributed hydrologic-land models in land use planning studies with water-dependent benefit functions.

3.1. Trade-offs between multiple competing objectives

The tradeoffs between 145 identified nondominated solutions are visualized in a parallel axis plot in Fig. 5. The objectives are plotted on the first five axes. The last two axes visualize the auxiliary variables representing the number of cells with land cover types not used in the calculation of any of the objective functions. The direction of preference for each objective is indicated with a black arrowhead positioned at the top of each axis.

Fig. 5 demonstrates that tradeoffs exist between all five objectives and different objectives are favoured by different land cover types. For example, generation of larger amounts of hydroelectric energy, which is proportional to total runoff volume, comes at the cost of lower food production, lower land cover diversity and lesser solar power generation potential. Land cover designs with high hydropower production are also prone to more flooding since land cover configurations that lead to large annual runoff volumes tend to also produce higher peak flows. The highest annual hydropower is produced when most of the land is allocated to grasslands due to grasslands having the lowest ET out of all four land cover types used in this study. A negative correlation exists between runoff and total bare soil area because, conversely to grasslands, this land use type has the highest ET out of the four land use types considered. Note, in the applied parameterization of bare soil evaporation, resistance to vapour transport in the soil is neglected, which results in high evaporation rates at the thermodynamic equilibrium of free water in contact with the

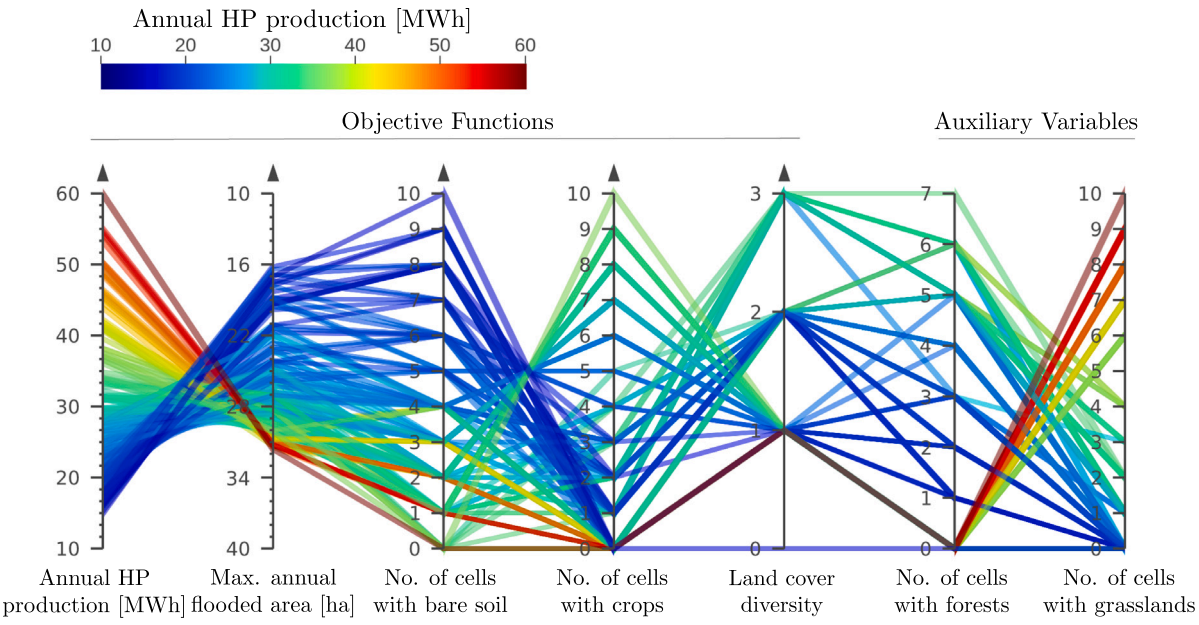

Fig. 5. Parallel axis plot visualizing trade-offs between the objective functions for 145 nondominated solutions. Black arrowhead at the top of each vertical axis indicates the direction of preference for the objective value.

atmosphere. Solutions with significant area allocated to crops, thus benefiting food production, are characterized by moderate hydropower generation, moderate to high flooding, and small to moderate solar power (SP) potential. Improving land cover diversity, by definition, requires a mix of all types of vegetation which have different properties and favour different objectives. Hence, solutions with high land cover diversity generate balanced quantities of solar power, hydropower and crops.

To gain a better insight into the topology of the Pareto optimal surface, the solutions were also plotted in a Cartesian coordinate system using three different projections in Fig. 6. The 2D projections in subplot (b) and subplot (c) illustrate, respectively, the shape of the relationship between hydropower production and the extent of flooding, and the relationship between the amount of bare soil and hydropower. The relationship between hydropower and the extent of flooding is monotonic and concave down with a plateau in the curve suggesting that above a certain threshold further increase in runoff does not produce higher peak flows. This suggests a presence of a cluster composed of combinations of land cover types which produce high overall runoffs but proportionally lower peak flows. This cluster is marked in the subplots as Cluster 1. Cluster 1 is composed of nondominated solutions representing the hillslope covered predominantly with grasslands with a small fraction of bare soil. Land cover diversity of one indicates absence of any other land cover types, i.e. forests or croplands. On the opposite side of the Pareto front lies Cluster 3 composed of non-dominated solutions generating the least runoff and producing the least flooding. These solutions represent designs with large area of bare soil with addition of croplands and forests, and favour solar power generation at the cost of lower land cover diversity, and hydropower and crop production. Cluster 2 represents intermediate land cover design scenarios which benefit all five objectives to similar degrees. Solutions in Cluster 2 thus have moderate land cover diversities and moderate hydropower, solar power, and food production potentials as a consequence of featuring a mix of several land cover types, each satisfying different objectives.

Interaction between land and groundwater depth is dependent on the vegetation/soil evaporation ratio resulting from an interplay of a number of vegetation-dependent parameters such as leaf area index (LAI) and root depth (RD). Since evaporation from soil and evapotranspiration through vegetation are driven by different processes, land uses with different vegetation/soil evaporation ratios exhibit different dynamic responses to changes in atmospheric conditions, such as rainfall, temperature, radiation or humidity. Dynamic response of a land use to rainfall will affect how much water is absorbed and evaporated vs how much recharges the groundwater system and contributes to river flow. The concave up shape of the curve in Fig. 6 can be explained by these differences. As grasslands have lower ET than croplands the amount of water retained in the subsurface in grassland-dominated catchments is higher, leading to larger overall runoff. However, since grasslands, compared to crops, evaporate proportionally more from soil than via transpiration, their response to high intensity short rainfalls is different. The subsurface under grasslands-dominated land is characterized with lower GW levels and lower shallow soil moisture. Consequently, in case of rainfall, less water recharges the groundwater thus producing moderate increase in river flow. Ultimately, the response of grasslands is less flashy than that of croplands.

The above results qualitatively agree, on a macroscopic scale, with the results of the earlier studies based on more aggregated models. In particular, the results corroborate the findings of Isik et al. (2013), Niu and Sivakumar (2014) who reported that hydrology of forest dominated areas was less flashy and with lower average flows whilst average and peak flow increased for pasture dominated areas. The results also agree with the findings of Mao and Cherkauer (2009) who reported the lowest spring total runoff in forest dominated areas due to higher annual ET whilst grasslands and croplands had higher spring total runoffs because of their lower ET losses. The outputs presented above result from aggregating spatially distributed results which can be explored further and unveil more information about the relationships between spatial arrangements of land cover and the catchment's behaviour.

3.2. Spatial distribution of land covers on the hillslope

The three clusters marked in Fig. 6 can also be found through visual inspection of the heatmaps in Fig. 7 and Fig. 8. These figures describe how land uses are distributed along the length of the hillslope. All five heatmaps can be inspected along the x-axis to observe how optimized land cover patterns change with each objective as well as along the y-axis to see land cover distribution along the hillslope. To aid the latter, the plots are divided into two regions in the y-direction, with the border between the two regions marked with two red pins on opposite sides

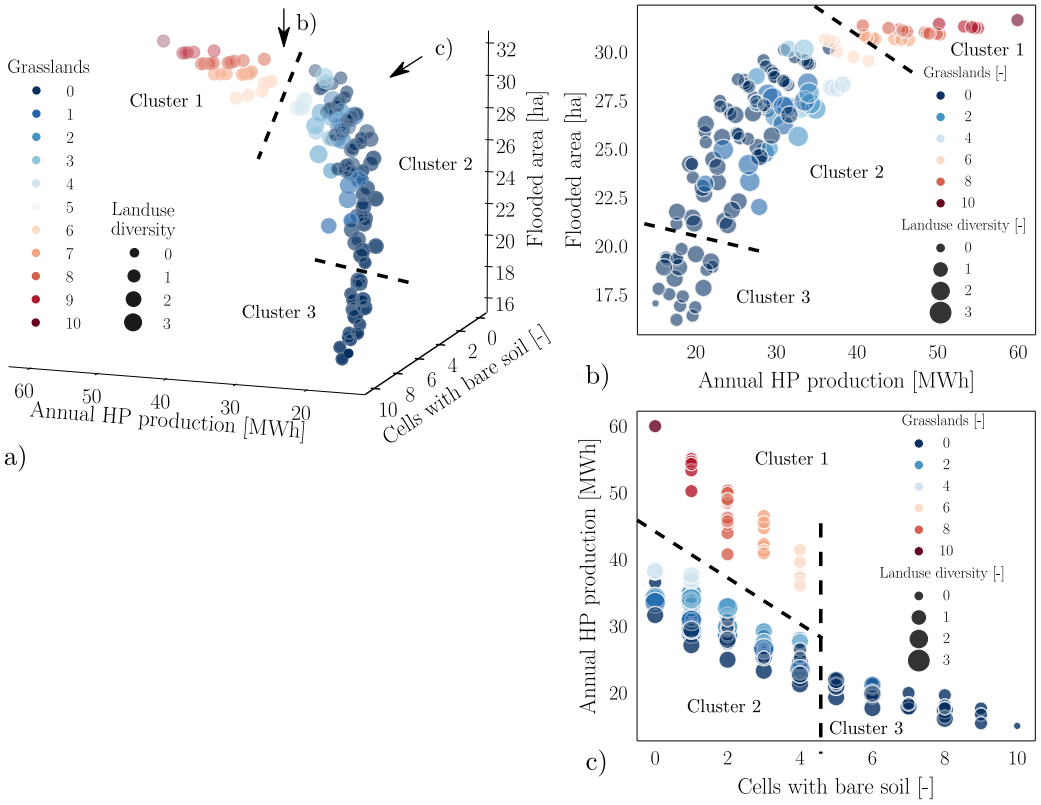

Fig. 6. Three-dimensional scatter plot of the five-dimensional Pareto set approximation constructed from non-dominated solutions (a) and two 2D projections of this Pareto set approximation visualizing (b) the relationship between hydropower production and flooded area and (c) locations of clusters in the nondominated solution set. The arrows in the top right corner of the 3D scatter plot indicate the directions of the two 2D projections.

of each heatmap. The upper region corresponds to Zone 3 in Fig. 2 in which groundwater level begins to fall below the maximum root zone depth, creating water-limited conditions suppressing ET for all vegetation types. The results in each heatmap are processed along both directions. Since this case-study is based on a synthetic 2D hillslope, the results cannot be directly transferred onto a full-scale catchment. However, they reflect the behaviour of the coupled land-hydrologic system including its plant functional types in ParFlow/CLM which were validated in previous studies. This study investigates what processes are responsible for the identified patterns in the solutions and the results can be used to provide an indication of potential behaviour of more complex computational domains representative of real-world catchments.

The heat maps constitute a complementary source of information to parallel axis and Pareto surface plots introduced in the previous section. As the nondominated solutions are individually sorted by the values of every objective function, they show how optimized spatial land cover allocations change as one objective is progressively favoured over the others. The heatmaps allow investigating each solution in a spatial dimension to answer questions such as whether (a) specific parts of the catchment favour certain land cover types; (b) certain land cover types should be positioned next to each other; (c) multiple solutions exist with the same aggregate land cover areas but different spatial allocations; and (d) a change in land cover in one isolated place within the catchment can significantly alter its behaviour. In Fig. 7 there are a number of solutions which have the same composition of land covers but produce different runoffs and/or peak flows depending on where the different land covers are placed within the hillslope.

Figs. 7 and 8 indicate that the preferred location for grasslands and croplands is in Zone 3. Placing these two land cover types, having the lowest ET out of all four land cover types considered in this study, in the part of the hillslope where ET is additionally water-limited, minimizes total ET, maximizes recharge, base flow and discharge, and thus maximizes hydropower production. Introduction of croplands additionally improves the agricultural production objective. For the selected objectives and land cover types, most efficient land cover designs include a mix of croplands, grasslands and bare soil. Bare soil tends to appear first in the lower sections of the hillslope in conjunction with grasslands and crops as, respectively, hydropower and food production objectives are gradually traded-off for solar power and for mitigating the risk of flooding.

Looking at Fig. 9 which shows the variability of mean annual WTDs per land cover type and cell, groundwater level under bare soil is the lowest out of all four land cover types considered as bare soil has the highest ET. Consequently, placing bare soil just upstream of grasslands and croplands creates a drop in the water level further down in the hillslope creating water-limited conditions for these two land cover types, ultimately producing overall lowest total ET - lower than if bare soil was placed at the very top of the hillslope. The information about the GW levels and its variability for different land cover arrangements becomes especially useful when groundwater levels are an important factor in land use optimization, e.g. when one or more objectives are related to water abstraction from the subsurface.

Since many solutions feature the same number of cells with bare soil, see upper subplot in Fig. 8], repeated solutions are sorted in the direction of decreasing runoff. As ET of bare soil is high due to the applied parameterization, and therefore, water level underneath the hillslope with predominantly bare soil cover, is low, mixing croplands and grasslands into catchments dominated by bare soil increases total runoff only negligibly. For this reason, the optimizer chooses instead to co-locate bare soil with forests which can evaporate large amounts of water due to their extensive root system. The preferred strategy is to improve flood mitigation objective whilst increasing land cover diversity. As the bare soil area gradually decreases, solutions begin

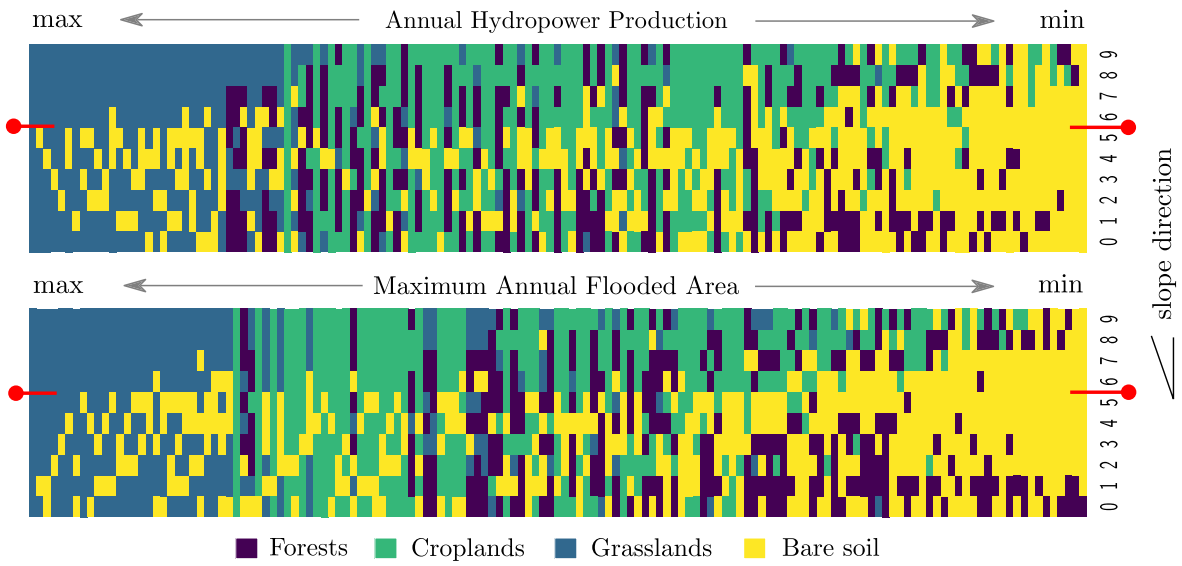

Fig. 7. Heatmaps showing land cover allocations on the hillslope for all nondominated solutions sorted by annual hydropower production (top) and maximum annual flooded area (bottom). The short red lines between Cell 5 and Cell 6 mark the location of the transition between Zones 1 and 2 and Zone 3 - see Fig. 2 for reference.

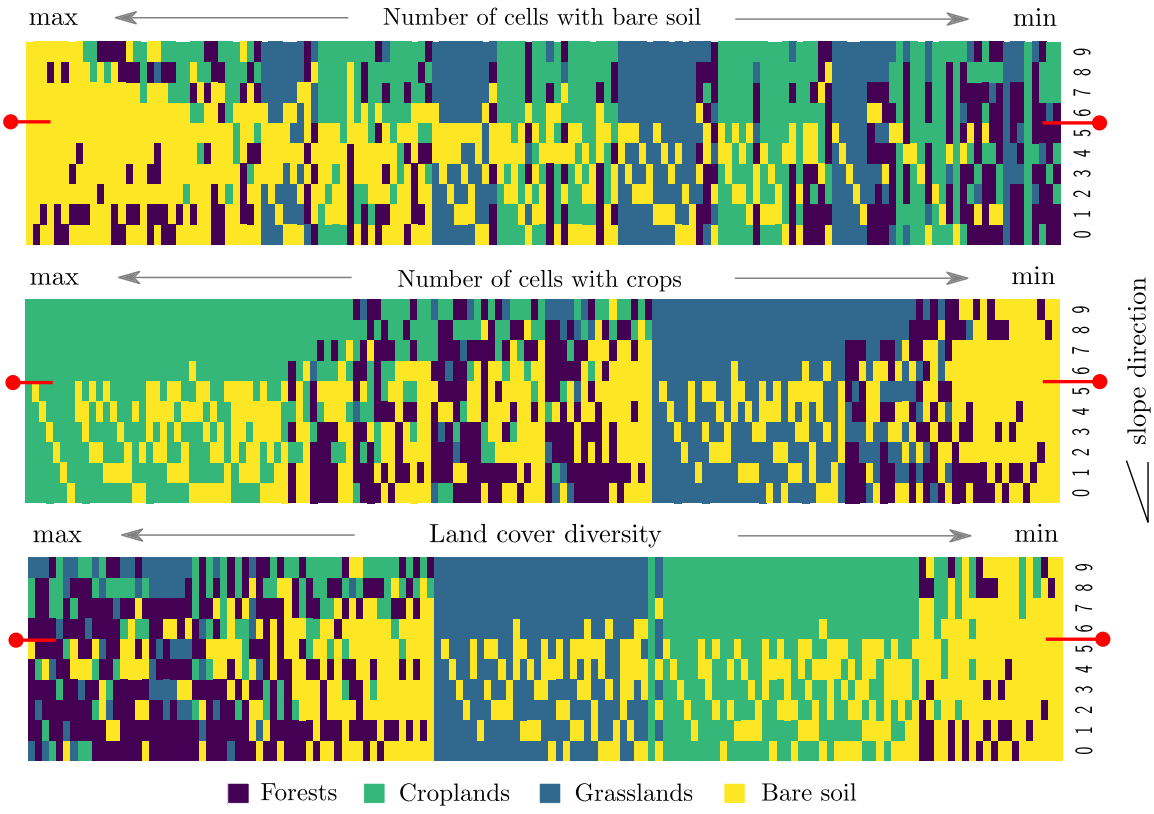

Fig. 8. Heatmaps showing land cover allocations on the hillslope for all nondominated solutions sorted, from top to bottom, by number of cells with bare soil, number of cells with crops, and land cover diversity. In cases where multiple solutions share the same value of the objective function, the solutions are ordered by hydropower in descending order. The short red lines between Cell 5 and Cell 6 mark the location of the transition between Zones 1 and 2 and Zone 3 - see Fig. 2 for reference.

to feature croplands which further improve land cover diversity and additionally, benefit the food production objective. Finally, a pattern emerges where initially bare soil is co-located with grasslands to benefit runoff and later, with croplands, which, although generate less runoff than grasslands, benefit agricultural food production objective. This pattern repeats in steps as the number of cells with bare soil is reduced one by one while solutions with equal areas of bare soil are sorted in the direction of decreasing hydropower production.

Croplands evaporate significantly less water than forests and bare soil, albeit more than grasslands. Therefore, land cover designs dominated by croplands tend to produce intermediate hydropower. Earlier results demonstrated that croplands produce higher peak flows with respect to total runoff than grasslands, i.e. lead to flashier runoff responses. What follows, croplands are co-located with bare soil in order to reduce peak flows and thus, the extent of flooding. If we investigate land cover allocations in the direction of decreasing agricultural

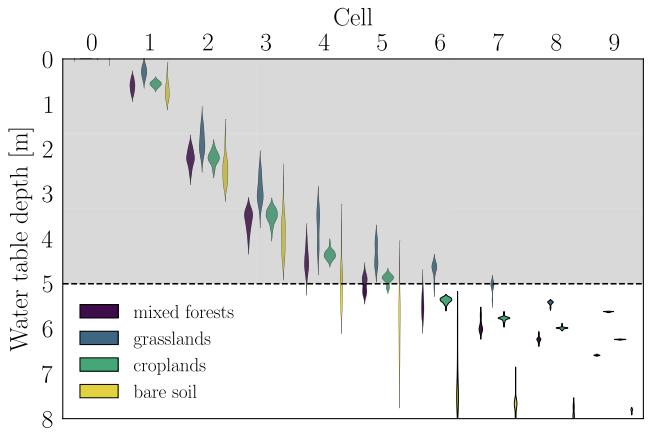

Fig. 9. Violin plot showing probability distributions of mean annual water depths in each cell for each land use type in the set of nondominated solutions. Grey shaded area represents the maximum root zone depth.

production, croplands initially cover an entire hillslope. Gradually, they are replaced with bare soil thus benefiting solar power and reducing the risk of flooding at the cost of food production. As previously, bare soil is preferably placed in the lower parts of the hillslope where ground water levels are at their highest, while grasslands tend to be positioned in the upper parts of the hillslope. Scenarios with lower fractions of croplands in the hillslope feature forests to increase land cover diversity.

It is intuitive that the scenarios with the highest land cover diversity scores feature a mixture of all land cover types. Interestingly, those scenarios are also abundant in forests. Inclusion of forests not only ensures reaching the maximum diversity score of 3 but also improves the flood control objective due to forests' high ET potential. Hence, land cover diversity and flood control objectives are, in this case, positively correlated.

The preference of a given land cover type over others with relation to the proximity to groundwater can be partly explained by looking at Fig. 10 that describes the relationship between ET and its soil and vegetation evaporation components vs. water table depth (WTD). While, on average, ET for the considered land use types follows the order: bare soil > mixed forests > croplands > grasslands, the relative differences between them are not constant alongside the hillslope. The benefit of choosing a certain land use type over another for a given objective may therefore be different in magnitude or even in sign, depending on where in the catchment the decision is made. For example, in the parts of the hillslope where groundwater levels are high, ET of bare soil exceeds that of a forest as shallow soil moisture dependent evaporation from land dominates over transpiration through stomatal apertures of leaves. However, once evaporation from land becomes limited by shallow soil moisture, ET from bare soil decreases sharply whilst ET of forests remain high as trees are still able to access ground water at lower levels via their root system. Consequently, if reduction of runoff is desired, the results suggest that bare soil should be placed in the lower parts of the catchment because this will lead to the highest increase of ET overall as well as relative to other land use types, in particular forests. Other mechanisms impacting spatial land cover allocations in a catchment include the effects of upstream decisions on the hydrologic conditions downstream via lateral flow, as discussed earlier in this section.

3.3. Effects of land cover distribution within solutions having the same land cover composition

The effects of varying the location of different land cover types on the hillslope on its hydrologic performance are shown in the left subfigure of Fig. 11. The figure describes the relationship between two objectives: the annual HP production and the maximum annual flooded area for solutions with equal land cover composition but different land cover arrangements. The remaining three objectives are invariant to land-cover arrangements as they depend on the total number of land covers and not on their positions. The figure shows up to 16% difference in annual HP production among solutions having the same land cover composition — see solutions with a mix of bare soil and grasslands. Maximum annual flooded area, which is proportional to peak flow, is less dependent on land cover arrangements in this example, albeit we can still observe differences up to 8%. These variations are mainly driven by the placement of, first and foremost, bare soil and to a lesser degree, forests, i.e. the vegetation types associated with largest ET. The right subfigure of Fig. 11 shows the histograms and kernel density estimates (KDEs) of the mean distance between each land cover and the river and corroborates that bare soil and forests are the two land cover types most spread along the hillslope, as indicated by their wide distributions. Both are also left skewed thus indicating the preference for allocating them in the lower part of the hillslope. On the other hand, grasslands and croplands have right-skewed distributions, indicating that their preferred placement is further up in the hillslope. Bare soil is the mostly featured land cover type in the set of nondominated solution, indicating that bare soil has the most utility, in our problem formulation, for optimally balancing the chosen objectives. Given land cover indices $j = 1, \ldots, 4$, the mean distance $\bar{d}_{l_j}$ between each land cover type l_j in kth nondominated solution $\mathbf{x}^{(k)}$ and the river has been calculated as the sum of indices i of cells with land cover l_j divided by the total number of cells with land cover l_j allocated in the hillslope. $\mathrm{card}(\cdot)$ is a set cardinality operator.

$$\bar{d}_{l_j} = \frac{\sum_{i=0}^{i=9} \left(i \mid x_i^{(k)} = l_j \right)}{\mathrm{card}\left(\{ x_i^{(k)} \in \mathbf{x}^{(k)} \mid x_i^{(k)} = l_j \} \right)} \tag{7}$$

In summary, the results show that in order to optimally balance the applied objectives, the location and combination of the different land covers types in the hillslope is important, as already reported in Warburton et al. (2012), Costa et al. (2003) and may be difficult to predict using expert knowledge due to nonlinear feedbacks of subsurface hydrology with the land processes and the lateral groundwater flow that are hard to envisage without detailed models. In the simulations, these results depend on the parameterization of evapotranspiration in the applied model and the representation of hydrology and hydrogeology of the hillslope or watershed.

3.4. Limitations and future research directions

The main limitation of this study is related to (a) the speed of execution of ParFlow/CLM and (b) the computational complexity and multi-dimensionality of multiobjective combinatorial land use optimization. This study showed that even for a rather simple catchment geometry, restricted pool of available land cover types, and short time horizons, the number of unction evaluations required by MOEA for convergence was large enough that the optimization study had to be run for 7-days on multi-processor architectures.

The first limitation could be mitigated by improving the manner in which coupled hydrologic/land and water resources models and MOEAs are spawned across multiple central processing units (CPUs) and graphics processing units (GPUs) and exchange data with each other. In this study, the exchange of data between ParFlow and Pywr happened via binary files which might have slowed down the simulation execution times by I/O bound file reading and writing processes. Another potential solution could involve researching numerical schemes for solving hydrologic and energy exchange flux equations that are stable for longer time steps than currently employed hourly step, thus reducing the number of computational time-steps required to run hydrologic simulations.

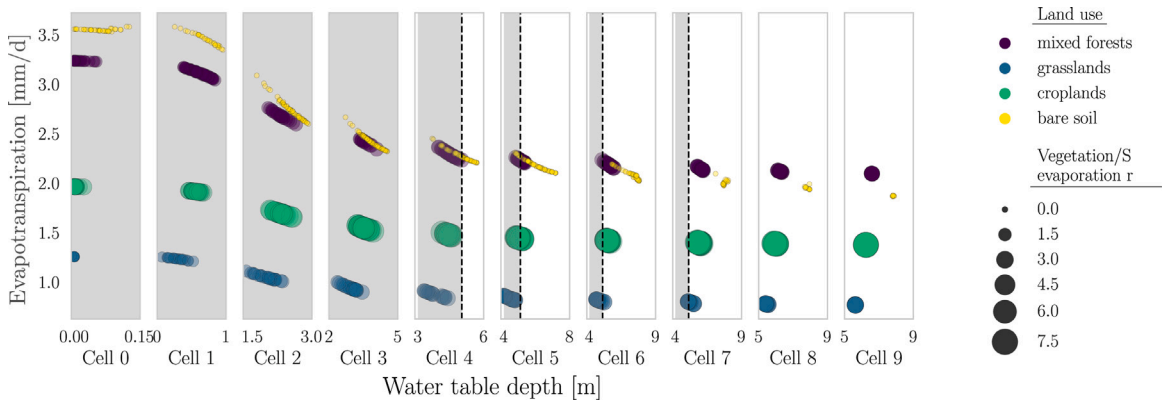

Fig. 10. Relationship between mean annual total evaporation and annual average water table depth in each cell and each land cover type obtained from the set of calculated 145 nondominated solutions. Grey shaded area represents the maximum root zone depth. Note that although the cells as shown as isolated systems, in fact they are physically linked via lateral subsurface flow from Cell 9 to Cell 0. The hydrologic state in each cell depends on the decisions made in the current cell and the upstream cells.

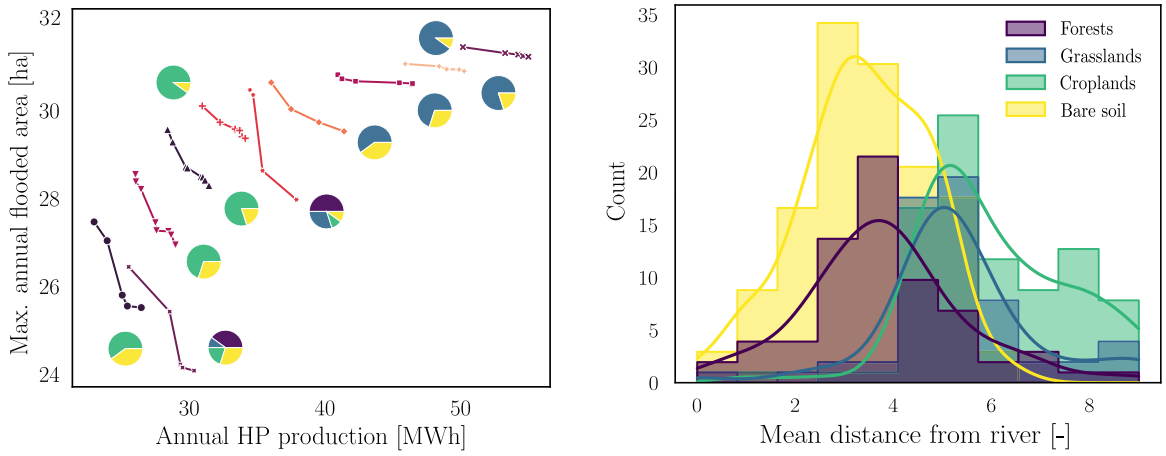

Fig. 11. Relationship between annual HP production and maximum annual flooded area among the nondominated solutions with the same land cover composition but different land cover arrangements (left) and distributions of land cover on the hillslope within the nondominated solution set (right). The river from which the distance is measured in the subfigure on the right, is represented on the hillslope as Cell 0. Land cover compositions are depicted in the left subfigure with pie-charts placed next to line plots.

The second barrier could be tackled at (a) the algorithmic level via development of custom algorithms specific to combinatorial land use optimization problems as well as (b) the choice and fine tuning best-suited existing algorithms. Application-specific MOEAs might include, e.g. custom crossover and mutation operators (Mohammadi et al., 2015) or additional geometric operators (García et al., 2017) that generate solutions with appropriate compactness, compatibility and contiguousness properties that satisfy feasibility requirements, specific to land use planning, directly within the algorithm. On the other hand, application of constraints within existing GAs could be implemented e.g. via application of penalty functions to degrade the fitness value of infeasible solutions or via incorporation of repair mechanisms for infeasible individuals (Cao et al., 2012).

A promising avenue towards increased scalability of the proposed framework is in learning surrogate, e.g. deep learning models, which can emulate the behaviour of models such as ParFlow/CLM at significantly higher speeds. The recent advancements in deep learning proved their applicability of solving high-dimensional partial differential equations, such fluid dynamic equations — see e.g. Morrison and Kutz (2022) and assisting with order reduction of highly-dimensional dynamic models (Baddoo et al., 2021).

4. Conclusion

This study demonstrated the benefits of using a mechanistic distributed land and hydrologic model combined with a water resources model for land use planning in multisector systems. The WEF land cover design framework attempts to consider the feedbacks between land and subsurface and the link between hydrology and water management. Although the study was designed as a proof-of-concept and carried out on a simplified hillslope model with homogeneous subsurface conditions, it retained the required subsurface flow complexity, including lateral flow. We hypothesize that the main findings related to impacts of land cover arrangements on Pareto-optimal solutions will also apply, in a qualitative sense, to more complex watersheds and we make suggestions for overcoming the computational challenges this would imply. Potential extensions to this framework could include (1) land cover planning with other water-related objectives, such as e.g. erosion sediment transport, (2) studies with bi-directional interactions between hydrologic and water resources, e.g., including diversions and ground water pumping, (3) studies with larger numbers of decision variables, e.g., for joint optimization of land cover and water management practices, such as hydroelectric reservoir operation, (4) analysis of impact of subsurface heterogeneity.

5. Supplementary material

The optimization results can be explored in an interactive manner and downloaded in CSV format from a web application at https://drawit-moea-results.onrender.com/.

CRediT authorship contribution statement

Tomasz Janus: Methodology, Formal analysis, Investigation, Visualization, Software, Writing – original draft, Writing – review & editing. **James Tomlinson:** Conceptualization, Software, Methodology. **Daniela Anghileri:** Conceptualization, Methodology, Investigation, Writing – review & editing. **Justin Sheffield:** Conceptualization. **Stefan Kollet:** Conceptualization, Methodology, Investigation, Writing – review & editing. **Julien J. Harou:** Conceptualization, Methodology, Writing – review & editing, Funding acquisition, Resources.

Declaration of competing interest

The authors declare that they have no known competing financial interests or personal relationships that could have appeared to influence the work reported in this paper.

Data availability

No data was used for the research described in the article.

Acknowledgements

J. Harou was funded through an Alexander von Humboldt Research Fellowship at the Jülich Forschungszentrum. The Natural Environment Research Council (NERC), UK provided funding through the 'Designing Resilient and Adaptable Water management-Integrated & Interactive Tools' (DRAW-IT) project (NE/S017305/1). Further funding was provided by the UK Research and Innovation (UKRI) Global Challenge Research Fund (GCRF), UK 'Future Design and Assessment of water-energy-food-environment Mega-Systems' (FutureDAMS) project (ES/P011373/1).

References

Ajami, H., McCabe, M.F., Evans, J.P., Stisen, S., 2014. Assessing the impact of model spin-up on surface water-groundwater interactions using an integrated hydrologic model. Water Resour. Res. 50 (3), 2636–2656. http://dx.doi.org/10.1002/2013WR014258, arXiv:https://agupubs.onlinelibrary.wiley.com/doi/pdf/10.1002/2013WR014258. URL https://agupubs.onlinelibrary.wiley.com/doi/abs/10.1002/2013WR014258.

Allen, R., 2005. Penman–monteith equation. In: Hillel, D. (Ed.), Encyclopedia of Soils in the Environment. Elsevier, Oxford, pp. 180–188. http://dx.doi.org/10.1016/B0-12-348530-4/00399-4, URL https://www.sciencedirect.com/science/article/pii/B0123485304003994.

Arcement, G.J., Schneider, V.R., 1989. Guide for selecting manning's roughness coefficients for natural channels and flood plains. Tech. Rep., Report, http://dx.doi.org/10.3133/wsp2339, URL http://pubs.er.usgs.gov/publication/wsp2339.

Arnold, J.G., Fohrer, N., 2005. SWAT2000: current capabilities and research opportunities in applied watershed modelling. Hydrol. Process. 19 (3), 563–572. http://dx.doi.org/10.1002/hyp.5611, arXiv:https://onlinelibrary.wiley.com/doi/pdf/10.1002/hyp.5611. URL https://onlinelibrary.wiley.com/doi/abs/10.1002/hyp.5611.

Ashby, S.F., Falgout, R.D., 1996. A parallel multigrid preconditioned conjugate gradient algorithm for groundwater flow simulations. Nucl. Sci. Eng. 124 (1), 145–159. http://dx.doi.org/10.13182/NSE96-A24230, arXiv:https://doi.org/10.13182/NSE96-A24230.

Baddoo, P.J., Herrmann, B., McKeon, B.J., Kutz, J.N., Brunton, S.L., 2021. Physics-informed dynamic mode decomposition (piDMD). http://dx.doi.org/10.48550/ARXIV.2112.04307, URL https://arxiv.org/abs/2112.04307.

Bearup, L.A., Maxwell, R.M., McCray, J.E., 2016. Hillslope response to insect-induced land-cover change: an integrated model of end-member mixing. Ecohydrology 9 (2), 195–203. http://dx.doi.org/10.1002/eco.1729, arXiv:https://onlinelibrary.wiley.com/doi/pdf/10.1002/eco.1729. URL https://onlinelibrary.wiley.com/doi/abs/10.1002/eco.1729.

Beven, K., 2007. Environmental Modelling: An Uncertain Future? first ed. CRC Press, http://dx.doi.org/10.1201/9781482288575.

Beven, K., 2019. Towards a methodology for testing models as hypotheses in the inexact sciences. Proc. Math. Phys. Eng. Sci. 475 (2224), 20180862.

Cao, K., Huang, B., Wang, S., Lin, H., 2012. Sustainable land use optimization using boundary-based fast genetic algorithm. Comput. Environ. Urban Syst. 36 (3), 257–269. http://dx.doi.org/10.1016/j.compenvurbsys.2011.08.001, URL https://www.sciencedirect.com/science/article/pii/S019897151100086X.

Choi, W., Deal, B.M., 2008. Assessing hydrological impact of potential land use change through hydrological and land use change modeling for the Kishwaukee River basin (USA). J. Environ. Manag. 88 (4), 1119–1130. http://dx.doi.org/10.1016/j.jenvman.2007.06.001, URL https://www.sciencedirect.com/science/article/pii/S0301479707001995.

Condon, L.E., Maxwell, R.M., 2013. Implementation of a linear optimization water allocation algorithm into a fully integrated physical hydrology model. Adv. Water Resour. 60, 135–147. http://dx.doi.org/10.1016/j.advwatres.2013.07.012, URL https://www.sciencedirect.com/science/article/pii/S0309170813001279.

Costa, M.H., Botta, A., Cardille, J.A., 2003. Effects of large-scale changes in land cover on the discharge of the Tocantins River, Southeastern Amazonia. J. Hydrol. 283 (1), 206–217. http://dx.doi.org/10.1016/s0022-1694(03)00267-1, URL https://www.sciencedirect.com/science/article/pii/S0022169403002671.

Dai, Y., Zeng, X., Dickinson, R.E., Baker, I., Bonan, G.B., Bosilovich, M.G., Denning, A.S., Dirmeyer, P.A., Houser, P.R., Niu, G., Oleson, K.W., Schlosser, C.A., Yang, Z.-L., 2003. The common land model. Bull. Am. Meteorol. Soc. 84 (8), 1013–1024. http://dx.doi.org/10.1175/BAMS-84-8-1013, URL https://journals.ametsoc.org/view/journals/bams/84/8/bams-84-8-1013.xml.

Deb, K., 2001. Multi-Objective Optimization using Evolutionary Algorithms. John Wiley & Sons.

Deb, K., Jain, H., 2014. An evolutionary many-objective optimization algorithm using reference-point-based nondominated sorting approach, part I: solving problems with box constraints. IEEE Trans. Evol. Comput. 18 (4), 577–601. http://dx.doi.org/10.1109/TEVC.2013.2281535.

Deb, K., Pratap, A., Agarwal, S., Meyarivan, T., 2002. A fast and elitist multiobjective genetic algorithm: NSGA-II. IEEE Trans. Evol. Comput. 6 (2), 182–197. http://dx.doi.org/10.1109/4235.996017.

Delgado, J., Llorens, P., Nord, G., Calder, I.R., Gallart, F., 2010. Modelling the hydrological response of a Mediterranean medium-sized headwater basin subject to land cover change: The Cardener River basin (NE Spain). J. Hydrol. 383 (1), 125–134. http://dx.doi.org/10.1016/j.jhydrol.2009.07.024, Water Quality and Assessment under Scarcity. Prospects and challenges in Mediterranean watersheds. URL https://www.sciencedirect.com/science/article/pii/S002216940900417X.

D'Odorico, P., Davis, K.F., Rosa, L., Carr, J.A., Chiarelli, D., Dell'Angelo, J., Gephart, J., MacDonald, G.K., Seekell, D.A., Suweis, S., Rulli, M.C., 2018. The global food-energy-water nexus. Rev. Geophys. 56 (3), 456–531. http://dx.doi.org/10.1029/2017RG000591, arXiv:https://agupubs.onlinelibrary.wiley.com/doi/pdf/10.1029/2017RG000591. URL https://agupubs.onlinelibrary.wiley.com/doi/abs/10.1029/2017RG000591.

Fowler, K., Jenkins, E., Ostrove, C., Chrispell, J., Farthing, M., Parno, M., 2015. A decision making framework with MODFLOW-FMP2 via optimization: Determining trade-offs in crop selection. Environ. Model. Softw. 69, 280–291. http://dx.doi.org/10.1016/j.envsoft.2014.11.031, URL https://www.sciencedirect.com/science/article/pii/S1364815214003624.

García, G.A., Rosas, E.P., García-Ferrer, A., Barrios, P.M., 2017. Multi-objective spatial optimization: sustainable land use allocation at sub-regional scale. Sustainability 9 (6), http://dx.doi.org/10.3390/su9060927, URL https://www.mdpi.com/2071-1050/9/6/927.

Guo, S., Zhang, F., Engel, B.A., Wang, Y., Guo, P., Li, Y., 2022. A distributed robust optimization model based on water-food-energy nexus for irrigated agricultural sustainable development. J. Hydrol. 606, 127394. http://dx.doi.org/10.1016/j.jhydrol.2021.127394, URL https://www.sciencedirect.com/science/article/pii/S002216942101444X.

Hadka, D., 2015. Platypus. A free and open source python library for multi-objective optimization. [Online], https://github.com/Project-Platypus/Platypus. (Accessed 20 November 2020).

He, M., Hogue, T.S., 2012. Integrating hydrologic modeling and land use projections for evaluation of hydrologic response and regional water supply impacts in semi-arid environments. Environ. Earth Sci. 65 (6), 1671–1685. http://dx.doi.org/10.1007/s12665-011-1144-3.

Hundecha, Y., Bárdossy, A., 2004. Modeling of the effect of land use changes on the runoff generation of a river basin through parameter regionalization of a watershed model. J. Hydrol. 292 (1), 281–295. http://dx.doi.org/10.1016/j.jhydrol.2004.01.002, URL https://www.sciencedirect.com/science/article/pii/S0022169404000125.

IGBP, 0000. URL http://www.igbp.net.

Isik, S., Kalin, L., Schoonover, J.E., Srivastava, P., Graeme Lockaby, B., 2013. Modeling effects of changing land use/cover on daily streamflow: An Artificial Neural Network and curve number based hybrid approach. J. Hydrol. 485, 103–112. http://dx.doi.org/10.1016/j.jhydrol.2012.08.032, Hydrology of peri-urban catchments: processes and modelling. URL https://www.sciencedirect.com/science/article/pii/S0022169412007111.

Jain, H., Deb, K., 2014. An evolutionary many-objective optimization algorithm using reference-point based nondominated sorting approach, part II: handling constraints and extending to an adaptive approach. IEEE Trans. Evol. Comput. 18 (4), 602–622. http://dx.doi.org/10.1109/TEVC.2013.2281534.

Jinja Templating Engine, 0000. URL https://jinja.palletsprojects.com/en/3.0.x/templates/.

Jones, J.E., Woodward, C.S., 2001. Newton–Krylov-multigrid solvers for large-scale, highly heterogeneous, variably saturated flow problems. Adv. Water Resour. 24 (7), 763–774. http://dx.doi.org/10.1016/S0309-1708(00)00075-0, URL http://www.sciencedirect.com/science/article/pii/S0309170800000750.

Julian, J.P., Gardner, R.H., 2014. Land cover effects on runoff patterns in eastern Piedmont (USA) watersheds. Hydrol. Process. 28 (3), 1525–1538. http://dx.doi.org/10.1002/hyp.9692, arXiv:https://onlinelibrary.wiley.com/doi/pdf/10.1002/hyp.9692. URL https://onlinelibrary.wiley.com/doi/abs/10.1002/hyp.9692.

Kollet, S.J., Maxwell, R.M., 2006. Integrated surface–groundwater flow modeling: A free-surface overland flow boundary condition in a parallel groundwater flow model. Adv. Water Resour. 29 (7), 945–958. http://dx.doi.org/10.1016/j.advwatres.2005.08.006, URL http://www.sciencedirect.com/science/article/pii/S0309170805002101.

Kollet, S.J., Maxwell, R.M., 2008. Capturing the influence of groundwater dynamics on land surface processes using an integrated, distributed watershed model. Water Resour. Res. 44 (2), http://dx.doi.org/10.1029/2007WR006004, arXiv:https://agupubs.onlinelibrary.wiley.com/doi/pdf/10.1029/2007WR006004. URL https://agupubs.onlinelibrary.wiley.com/doi/abs/10.1029/2007WR006004.

Kuffour, B.N.O., Engdahl, N.B., Woodward, C.S., Condon, L.E., Kollet, S., Maxwell, R.M., 2020. Simulating coupled surface–subsurface flows with ParFlow v3.5.0: capabilities, applications, and ongoing development of an open-source, massively parallel, integrated hydrologic model. Geosci. Model Dev. 13 (3), 1373–1397. http://dx.doi.org/10.5194/gmd-13-1373-2020, URL https://gmd.copernicus.org/articles/13/1373/2020/.

Lautenbach, S., Volk, M., Strauch, M., Whittaker, G., Seppelt, R., 2013. Optimization-based trade-off analysis of biodiesel crop production for managing an agricultural catchment. Environ. Model. Softw. 48, 98–112. http://dx.doi.org/10.1016/j.envsoft.2013.06.006, URL https://www.sciencedirect.com/science/article/pii/S1364815213001424.

Li, M., Zhao, L., Zhang, C., Liu, Y., Fu, Q., 2022. Optimization of agricultural resources in water-energy-food nexus in complex environment: A perspective on multienergy coordination. Energy Convers. Manage. 258, 115537. http://dx.doi.org/10.1016/j.enconman.2022.115537, URL https://www.sciencedirect.com/science/article/pii/S0196890422003338.

Mao, D., Cherkauer, K.A., 2009. Impacts of land-use change on hydrologic responses in the Great Lakes region. J. Hydrol. 374 (1), 71–82. http://dx.doi.org/10.1016/j.jhydrol.2009.06.016, URL https://www.sciencedirect.com/science/article/pii/S0022169409003229.

Markovich, K.H., Maxwell, R.M., Fogg, G.E., 2016. Hydrogeological response to climate change in alpine hillslopes. Hydrol. Process. 30 (18), 3126–3138. http://dx.doi.org/10.1002/hyp.10851, arXiv:https://onlinelibrary.wiley.com/doi/pdf/10.1002/hyp.10851. URL https://onlinelibrary.wiley.com/doi/abs/10.1002/hyp.10851.

Maxwell, R.M., Miller, N.L., 2005. Development of a coupled land surface and groundwater model. J. Hydrometeorol. 6 (3), 233–247. http://dx.doi.org/10.1175/JHM422.1, arXiv:https://journals.ametsoc.org/jhm/article-pdf/6/3/233/4148276/jhm422_1.pdf.

McColl, C., Aggett, G., 2007. Land-use forecasting and hydrologic model integration for improved land-use decision support. J. Environ. Manag. 84 (4), 494–512. http://dx.doi.org/10.1016/j.jenvman.2006.06.023.

Mikkelson, K.M., Maxwell, R.M., Ferguson, I., Stednick, J.D., McCray, J.E., Sharp, J.O., 2013. Mountain pine beetle infestation impacts: modeling water and energy budgets at the hill-slope scale. Ecohydrology 6 (1), 64–72. http://dx.doi.org/10.1002/eco.278, arXiv:https://onlinelibrary.wiley.com/doi/pdf/10.1002/eco.278. URL https://onlinelibrary.wiley.com/doi/abs/10.1002/eco.278.

Mohammadi, M., Nastaran, M., Sahebgharani, A., 2015. Sustainable spatial land use optimization through non-dominated sorting genetic algorithm-II (NSGAII): (case study: baboldasht district of isfahan). Indian J. Sci. Technol. 8 (S3), 118–129. http://dx.doi.org/10.17485/ijst/2015/v8iS3/60700.

Monin, A., Obukhov, A., 1954. Basic laws of turbulent mixing in the surface layer of the atmosphere. Contrib. Geophys. Inst. Acad. Sci. 24, 163–187, USSR.

Morrison, M., Kutz, J.N., 2022. Solving nonlinear ordinary differential equations using the invariant manifolds and koopman eigenfunctions. http://dx.doi.org/10.48550/ARXIV.2208.08529, URL https://arxiv.org/abs/2208.08529.

MPI4PY, 0000. URL https://mpi4py.readthedocs.io/en/stable/.

Niu, J., Sivakumar, B., 2014. Study of runoff response to land use change in the East River basin in South China. Stoch. Environ. Res. Risk Assess. 28 (4), 857–865. http://dx.doi.org/10.1007/s00477-013-0690-5.

Oleson, K., Lawrence, D., Bonan, G., Flanner, M., Kluzek, E., Lawrence, P., Levis, S., Swenson, S., Thornton, P., Dai, A., Decker, M., Dickinson, R., Feddema, J., Heald, C., Hoffman, F., Lamarque, J.-F., Mahowald, N., Niu, G.-Y., Qian, T., Randerson, J., Running, S., Sakaguchi, K., Slater, A., Stockli, R., Wang, A., Yang, Z.-L., Zeng, X., Zen, X., 2010. Technical Description of version 4.0 of the Community Land Model (CLM). NCAR Technical Note NCAR/TN-478+STR, O, National Center for Atmospheric Research, Boulder, C, p. 257.

Öztürk, M., Copty, N.K., Saysel, A.K., 2013. Modeling the impact of land use change on the hydrology of a rural watershed. J. Hydrol. 497, 97–109. http://dx.doi.org/10.1016/j.jhydrol.2013.05.022, URL https://www.sciencedirect.com/science/article/pii/S0022169413003892.

Penman, H.L., Keen, B.A., 1948. Natural evaporation from open water, bare soil and grass. Proc. R. Soc. Lond. Ser A. Math. Phys. Sci. 193 (1032), 120–145. http://dx.doi.org/10.1098/rspa.1948.0037, arXiv:https://royalsocietypublishing.org/doi/pdf/10.1098/rspa.1948.0037. URL https://royalsocietypublishing.org/doi/abs/10.1098/rspa.1948.0037.

Penn, C.A., Bearup, L.A., Maxwell, R.M., Clow, D.W., 2016. Numerical experiments to explain multiscale hydrological responses to mountain pine beetle tree mortality in a headwater watershed. Water Resour. Res. 52 (4), 3143–3161. http://dx.doi.org/10.1002/2015WR018300, arXiv:https://agupubs.onlinelibrary.wiley.com/doi/pdf/10.1002/2015WR018300. URL https://agupubs.onlinelibrary.wiley.com/doi/abs/10.1002/2015WR018300.

Ras, G., Xie, N., van Gerven, M., Doran, D., 2020. Explainable deep learning: a field guide for the uninitiated. http://dx.doi.org/10.48550/ARXIV.2004.14545, URL https://arxiv.org/abs/2004.14545.

Reed, P., Hadka, D., Herman, J., Kasprzyk, J., Kollat, J., 2013. Evolutionary multiobjective optimization in water resources: The past, present, and future. Adv. Water Resour. 51, 438–456. http://dx.doi.org/10.1016/j.advwatres.2012.01.005.

Ren, H., Liu, B., Zhang, Z., Li, F., Pan, K., Zhou, Z., Xu, X., 2022. A water-energy-food-carbon nexus optimization model for sustainable agricultural development in the Yellow River Basin under uncertainty. Appl. Energy 326, 120008. http://dx.doi.org/10.1016/j.apenergy.2022.120008, URL https://www.sciencedirect.com/science/article/pii/S030626192201265X.

Richards, D., Lin, H.-C., Cheng, H., Zhang, F., Huang, G., Edris, E., Yeh, G., 2005. A first-principle, physics-based watershed model: WASH123D.

Seck, A., Welty, C., Maxwell, R.M., 2015. Spin-up behavior and effects of initial conditions for an integrated hydrologic model. Water Resour. Res. 51 (4), 2188–2210. http://dx.doi.org/10.1002/2014WR016371, arXiv:https://agupubs.onlinelibrary.wiley.com/doi/pdf/10.1002/2014WR016371. URL https://agupubs.onlinelibrary.wiley.com/doi/abs/10.1002/2014WR016371.

Serafini, P., 1987. Some considerations about computational complexity for multi objective combinatorial problems. In: Jahn, J., Krabs, W. (Eds.), Recent Advances and Historical Development of Vector Optimization. Springer Berlin Heidelberg, Berlin, Heidelberg, pp. 222–232.

Sheikh, V., Salmani, H., Salman Mahiny, A., Ownegh, M., Fathabadi, A., 2021. Land use optimization through bridging multiobjective optimization and multicriteria decision-making models (case study: Tilabad Watershed, Golestan Province, Iran). Nat. Resour. Model. 34 (2), e12301. http://dx.doi.org/10.1111/nrm.12301, arXiv:https://onlinelibrary.wiley.com/doi/pdf/10.1111/nrm.12301. URL https://onlinelibrary.wiley.com/doi/abs/10.1111/nrm.12301.

Shen, C., Phanikumar, M.S., 2010. A process-based, distributed hydrologic model based on a large-scale method for surface–subsurface coupling. Adv. Water Resour. 33 (12), 1524–1541. http://dx.doi.org/10.1016/j.advwatres.2010.09.002, URL https://www.sciencedirect.com/science/article/pii/S0309170810001569.

Siriwardena, L., Finlayson, B., McMahon, T., 2006. The impact of land use change on catchment hydrology in large catchments: The Comet River, Central Queensland, Australia. J. Hydrol. 326 (1), 199–214. http://dx.doi.org/10.1016/j.jhydrol.2005.10.030, URL https://www.sciencedirect.com/science/article/pii/S0022169405005639.

Tomlinson, J., Arnott, J., Harou, J., 2020. A water resource simulator in Python. Environ. Model. Softw. 126, 104635. http://dx.doi.org/10.1016/j.envsoft.2020.104635, URL http://www.sciencedirect.com/science/article/pii/S1364815219307133.

Tong, S.T., Sun, Y., Ranatunga, T., He, J., Yang, Y.J., 2012. Predicting plausible impacts of sets of climate and land use change scenarios on water resources. Appl. Geogr. 32 (2), 477–489. http://dx.doi.org/10.1016/j.apgeog.2011.06.014, URL https://www.sciencedirect.com/science/article/pii/S0143622811001305.

Warburton, M.L., Schulze, R.E., Jewitt, G.P., 2012. Hydrological impacts of land use change in three diverse South African catchments. J. Hydrol. 414–415, 118–135. http://dx.doi.org/10.1016/j.jhydrol.2011.10.028, URL https://www.sciencedirect.com/science/article/pii/S0022169411007529.

Wijesekara, G., Gupta, A., Valeo, C., Hasbani, J.-G., Qiao, Y., Delaney, P., Marceau, D., 2012. Assessing the impact of future land-use changes on hydrological processes in the Elbow River watershed in southern Alberta, Canada. J. Hydrol. 412–413, 220–232. http://dx.doi.org/10.1016/j.jhydrol.2011.04.018, Hydrology Conference 2010. URL https://www.sciencedirect.com/science/article/pii/S0022169411002587.

Yang, Y., Li, Y., Huang, Q., Xia, J., Li, J., 2023. Surrogate-based multiobjective optimization to rapidly size low impact development practices for outflow capture. J. Hydrol. 616, 128848. http://dx.doi.org/10.1016/j.jhydrol.2022.128848, URL https://www.sciencedirect.com/science/article/pii/S0022169422014184.

Yue, Q., Zhang, F., Wang, Y., Zhang, X., Guo, P., 2021. Fuzzy multi-objective modelling for managing water-food-energy-climate change-land nexus towards sustainability. J. Hydrol. 596, 125704. http://dx.doi.org/10.1016/j.jhydrol.2020.125704, URL https://www.sciencedirect.com/science/article/pii/S0022169420311653.